Supplementary Materials for

Hidden Interactions in Financial Markets

Stavros K. Stavroglou, Athanasios A. Pantelous, H. Eugene Stanley, Konstantin M. Zuev

This PDF file includes:

Other Supplementary Materials for this manuscript include the following:

SI Video

www.pnas.org/cgi/doi/10.1073/pnas.1819449116

Materials and Methods

Notation

Variable	Description
E	The embedding dimension of the state space that engulfs the dynamical system under study.
d_M	The embedding dimension of the dynamical system as formed into an attractor $\boldsymbol{M}$ by the system's trajectories where $d_M \leq E$.
t	Denotes time measured in time steps $t_1, t_2, t_3, \ldots$ (e.g. days, weeks, months)
τ	The time lag we use to reconstruct a shadow attractor.
L	The time series length, also called library of the time series.
$\boldsymbol{M}$	The attractor consisting of all trajectories and possible states $\underline{x}(t)$ of the system. $\boldsymbol{M}$ is a d-dimensional attractor embedded in an E-dimensional state space ($d_M \leq E$). The state space contains the manifold and its dynamics and consists of the original E Cartesian coordinates (fundamental variables) of the system.
$m(t)$	The point (vector) on $\boldsymbol{M}$ representing the state of the system at time t.
X, Y	State variables of the system that operate as a function which map points from $\boldsymbol{M}$ to a real-valued scalar. X and Y may correspond to Cartesian coordinates of the actual E-dimensional state space containing $\boldsymbol{M}$.
$\{X\}, \{Y\}$	The time series corresponding to the values of variable X evolving through time. Thus, $\{X\}$ can be thought of as a serial projection of dynamics occurring on some manifold $\boldsymbol{M}$ onto a specific coordinate axis, X, recording displacements along that dimension through time.
$\boldsymbol{M_X}, \boldsymbol{M_Y}$	The shadow attractors reconstructed using time lags of $\{X\}$ and $\{Y\}$ respectively.
$x(t), y(t)$	The points (vectors) on $\boldsymbol{M_X}$ and $\boldsymbol{M_Y}$ respectively corresponding to the state of the system at time t.
$\boldsymbol{NN_X}, \boldsymbol{NN_Y}$	Local neighborhoods, i.e., collections of nearest neighbors on $\boldsymbol{M_X}$ and $\boldsymbol{M_Y}$ respectively based on some metric distance. In our paper we use Manhattan distance (L_1)
$NN_{x(t)}, NN_{y(t)}$	Nearest neighbors of points $x(t)$ and $y(t)$ respectively.
$\widehat{NN_{x(t)}}, \widehat{NN_{y(t)}}$	Estimated nearest neighbors through corresponding time indices (See PC algorithm).
$\boldsymbol{P_X}, \boldsymbol{P_Y}$	The average patterns, also called signatures, that represent local neighborhoods of $\boldsymbol{NN_X}$ and $\boldsymbol{NN_Y}$ and respectively. See equations S1, S2, S6, S7.
$P_{x(t)}, P_{y(t)}$	The average patterns (signatures) of $NN_{x(t)}$ and $NN_{y(t)}$ respectively.
$\widehat{P_{x(t)}}, \widehat{P_{y(t)}}$	The estimated average patterns (signatures) of $\widehat{NN_{x(t)}}$ and $\widehat{NN_{y(t)}}$ respectively.

Theoretical foundations of our method

In this section, we demonstrate the mathematical foundations of our treatment, and the details of extracting the nature of causality from time series. Our algorithm is primarily inspired by the theory of symbolic dynamics which was formally introduced by Morse and Hedlund[17] and further adapted for time series by Bandt and Pompe[34, 35]. Another important ingredient for our algorithm is dynamical systems theory[36] and especially attractor reconstruction[18].

Let us consider a discrete dynamical system that temporally evolves in an E-dimensional state space ($E \in \mathbb{N}$). Unless the system is completely stochastic, the orbits of its points will assemble into a d-dimensional attractor ($d_M \leq E$) $\boldsymbol{M}$. Let X be a state variable of the system that operates as a function which maps points from $\boldsymbol{M}$ to a real-valued scalar. Thus X can be measured through this mapping as a time series $\{X\}=\{X(1), \ldots, X(L)\}$ that records the orbits of points in $\boldsymbol{M}$. L is the time series length. By invoking the theory of time-delayed embedding, the E time-lagged (with lag = $\tau \in \mathbb{N}$) values of $\{X\}$ spawn vectors ($x(t)=<X(t), X(t\text{-}\tau), \ldots, X(t\text{-}(E\text{-}1)\tau)>$) which can be used to create a diffeomorphically reconstructed attractor $\boldsymbol{M_X}$ of the original attractor $\boldsymbol{M}$ [18, 19, 37, 38, 39]. Furthermore, an intrinsic feature of delayed-coordinate embedding is that points $x(t)$ on $\boldsymbol{M_X}$ map 1:1 to points $m(t)$ on $\boldsymbol{M}$ and local neighborhoods on $\boldsymbol{M_X}$ map to local neighborhoods on $\boldsymbol{M}$ [18, 19].

Let us now consider another state variable of the system Y. Since X and Y originate from the same dynamical system they are dynamically coupled and as a consequence contemporaneous neighborhoods on $\boldsymbol{M_X}$ and $\boldsymbol{M_Y}$ will map to each other[13, 18, 19, 37, 38, 39]. PC focuses on the symbolic dynamics (patterns) of the neighborhoods in $\boldsymbol{M_X}$ and $\boldsymbol{M_Y}$, and examines how consistently, average patterns $\boldsymbol{P_X}$ (signatures) in local neighborhoods $\boldsymbol{NN_X}$ of $\boldsymbol{M_X}$ correspond to average patterns $\boldsymbol{P_Y}$ (signatures) in contemporaneous neighborhoods $\boldsymbol{NN_Y}$ of $\boldsymbol{M_Y}$.

Determining the nature of causality

To establish the nature of causality from a time series X to a time series Y (similarly from Y to X), first both $\boldsymbol{M_X}$ and $\boldsymbol{M_Y}$ are created from time-delayed vectors of X and Y. Then, for each point $y(t)$ in $\boldsymbol{M_Y}$ we extract the average pattern $P_{y(t)}$ from its nearest neighbors $NN_{y(t)}$ and from them we estimate the contemporaneous average pattern $\widehat{P_{x(t)}}$. The strength of causality is determined by the overall accuracy percentage between the estimated $\widehat{P_{x(t)}}$ and the actual $P_{x(t)}$. Regarding the nature of causality, if the correspondence is consistent between same patterns ($\boldsymbol{P_X}$ same to $\boldsymbol{P_Y}$) then

positive causality defines the relationship of X and Y, whereas if opposite patterns are dominantly coupled (over same ones) then negative causality is the case.

In our paradigm, the patterns we define for E=2 are: i) ↗: $X(t\text{-}\tau) < X(t)$, ii) →: $X(t\text{-}\tau) = X(t)$, iii) ↘: $X(t\text{-}\tau) > X(t)$ and these cover all the possible temporal patterns that characterize time series. Furthermore, for E=3 we define i) ↗↗: $X(t\text{-}2\tau) < X(t\text{-}\tau) < X(t)$, ii) →↗: $X(t\text{-}2\tau) = X(t\text{-}\tau) < X(t)$, iii) ↘↗: $X(t\text{-}2\tau) > X(t\text{-}\tau) < X(t)$, iv) ↗→: $X(t\text{-}2\tau) < X(t\text{-}\tau) = X(t)$, v) →→: $X(t\text{-}2\tau) = X(t\text{-}\tau) = X(t)$, vi) ↘→: $X(t\text{-}2\tau) > X(t\text{-}\tau) = X(t)$, vii) ↗↘: $X(t\text{-}2\tau) < X(t\text{-}\tau) > X(t)$, viii) →↘: $X(t\text{-}2\tau) = X(t\text{-}\tau) > X(t)$, ix) ↘↘: $X(t\text{-}2\tau) > X(t\text{-}\tau) < X(t)$. The expansion on E=4 and beyond is plausibly derived in the same rationale.

There are cases however when persistent correspondence of patterns is confirmed through PC, yet the patterns are neither similar nor opposite (e.g. patterns of the form ↘↗ in X causing patterns of the form ↗↗ in Y), in such cases (which become abundant as E increases) we characterize this unclear nature of causality as dark (in a same manner that dark matter is defined in the universe [40]). For a complete blueprint on how to understand the nature of causality see Tables S1 and S2.

Remark on dark causality

Up until now scientific literature has concentrated on the obvious duality of interactions, i.e., positive/negative correlations[8], positively/negatively cointegrated time series[11] and positive/negative nonlinear interactions[14]. However, through the lens of PC we discover a third form of interactions which classify as neither positive nor negative. For example, interactions in E = 4 such as pattern ↗↗↗↗ in X consistently causing pattern ↘↗↘↗ in Y can be described as: successive increases in X cause oscillations in Y. Such a form of causality from X to Y is neither positive nor negative, yet it is possible to exist.

Signature

In order to express a representation of the dominant dynamics in a spatio-temporal neighborhood on a given attractor ***M*** first we calculate the weighted average (see example below) of the patterns corresponding to the nearest neighbors ***NN***. The calculation of the weights in PC algorithm is done according to equation S3 below. Then we characterize as signature the pattern ***P*** which emerges from that weighted average.

For example, let us have four patterns:

- $s_1 =$ ↗↗ = (0.32, 0.45), with corresponding weight, $w_1 = 0.91$.
- $s_2 =$ ↘↗ = (-0.11, 0.51), with corresponding weight, $w_2 = 0.54$.
- $s_3 =$ ↗↗ = (0.13, 0.19), with corresponding weight, $w_3 = 0.82$.
- $s_4 =$ ↗↘ = (0.05, -0.08), with corresponding weight, $w_4 = 0.69$.

The weighted average in our example is:

$$S = \sum_{i=1}^{4} w_i s_i = 0.91 * (0.32, 0.45) + 0.54 * (-0.11, 0.51) + 0.82 * (0.13, 0.19) + 0.69 * (0.05, -0.08) = (0.3729, 0.7855)$$

Thus, the emergent average pattern is the signature of S:

$$\boldsymbol{P} = signature(S) = ↗↗$$

PC Algorithm

Consider two time series of length L, $\{X\}=\{X(1), \ldots, X(L)\}$ and $\{Y\}=\{Y(1), \ldots, Y(L)\}$. Initially we derive an optimal combination of embedding dimension E and time delay τ. Optimal in our case would be with the least false nearest neighbors, given that our method relies heavily on neighborhood information. For that purpose, we use the False First Nearest Neighbor algorithm[41] which calculates an optimal combination of both embedding dimension E and proper time delay τ simultaneously.

Then we retrieve the shadow attractors $\boldsymbol{M_X}$ and $\boldsymbol{M_Y}$ by using the lagged-coordinate vectors $x(t)=<X(t), X(t-\tau), ..., X(t-(E-1)\tau)>$ and $y(t)=<Y(t), Y(t-\tau), ..., Y(t-(E-1)\tau)>$ for $t = 1+(E-1)\tau$ to $t = L$. To calculate PC from X to Y (similarly from Y to X), for each point $y(t)$ in $\boldsymbol{M_Y}$ we find its $E+1$ nearest neighbors $NN_{y(t)}$, which is the minimum number of points needed for a bounded simplex in an E-dimensional space. From these $E+1$ nearest neighbors we need to keep three pieces of information: i) their time indexes $t_{y_1}, \ldots, t_{y_{E+1}}$, ii) their Manhattan (L1) distance from $y(t)$, and iii) their temporal patterns as described in the previous section. As a next step, we use the aforementioned pieces of information to estimate or "predict" the average contemporaneous pattern of $x(t)$. To do this first we calculate the average pattern (signature) $P_{y(t)}$:

$$P_{y(t)} = signature\left(S_{y(t)}\right),\ S_{y(t)} \in \mathbb{R}^E, \tag{S1}$$

where

$$S_{y(t)} = \sum_{j=1}^{E+1} w_j^y s_j^y\ , w_j^y \in [0,1], s_j^y \in \mathbb{R}^E, \text{ for all } NN_{y(t)}, \tag{S2}$$

$$w_j^y = \frac{e^{-d(y(t),y(t_j))}}{\sum_j e^{-d(y(t),y(t_j))}}\ , d\text{: Manhattan distance} \tag{S3}$$

$$s_j^y = \left(\frac{y_j^{(2)} - y_j^{(1)}}{y_j^{(1)}}, \ldots, \frac{y_j^{(E+1)} - y_j^{(E)}}{y_j^{(E)}}\right), y_j \in \mathbb{R}, \tag{S4}$$

$$y\left(t_j\right) = \left(Y\left(t_j\right), Y\left(t_j - \tau\right), \ldots, Y\left(t_j - (E-1)\tau\right)\right) = \left(y_j^{(1)}, \ldots, y_j^{(E+1)}\right), Y \in \mathbb{R}, \tag{S5}$$

Then we estimate (i.e., predict) the mutual neighbors that correspond to $x(t)$ (contemporaneous to $y(t)$) by using the time indices of $y(t)$'s nearest neighbors: $\widehat{NN_{x(t)}} = x_{t_{y_1}}, \ldots, x_{t_{y_{E+1}}}$. We calculate similarly the "predicted" average pattern $\widehat{P_{x(t)}}$ as follows:

$$\widehat{P_{x(t)}} = signature\left(\widehat{S_{x(t)}}\right), \widehat{S_{x(t)}} \in \mathbb{R}^E, \tag{S6}$$

where

$$\widehat{S_{x(t)}} = \sum_{j=1}^{E+1} w_j^y s_j^{\hat{x}}\ , w_j^y \in [0,1], s_j^{\hat{x}} \in \mathbb{R}^E, \text{ for all } \widehat{NN_{x(t)}}, \tag{S7}$$

$$s_j^{\hat{x}} = \left(\frac{\hat{x}_j^{(2)} - \hat{x}_j^{(1)}}{\hat{x}_j^{(1)}}, \ldots, \frac{\hat{x}_j^{(E+1)} - \hat{x}_j^{(E)}}{\hat{x}_j^{(E)}}\right), \hat{x}_j \in \mathbb{R}, \tag{S8}$$

$$\hat{x}\left(t_j\right) = \left(\hat{X}\left(t_{y_1}\right), \hat{X}\left(t_{y_2}\right), \ldots, \hat{X}\left(t_{y_{E+1}}\right)\right) = \left(\hat{x}_j^{(1)}, \ldots, \hat{x}_j^{(E+1)}\right),\ \hat{X} \in \mathbb{R}, \tag{S9}$$

Finally, we calculate the real average pattern $P_{x(t)}$ from the actual nearest neighbors $\boldsymbol{NN_{x(t)}}$ of $x(t)$ to verify the estimation from Eq. S6:

$$P_{x(t)} = signature\left(S_{x(t)}\right),\ S_{x(t)} \in \mathbb{R}^E, \tag{S10}$$

where

$$S_{x(t)} = \sum_{j=1}^{E+1} w_j^x s_j^x\ , w_j^x \in [0,1], s_j^x \in \mathbb{R}^E, \text{ for all } NN_{x(t)}, \tag{S11}$$

$$w_j^x = \frac{e^{-d(x(t),x(t_j))}}{\sum_j e^{-d(x(t),x(t_j))}}\ , d\text{: Manhattan distance} \tag{S12}$$

$$s_j^x = \left(\frac{x_j^{(2)} - x_j^{(1)}}{x_j^{(1)}}, \ldots, \frac{x_j^{(E+1)} - x_j^{(E)}}{x_j^{(E)}}\right), x_j \in \mathbb{R}, \quad \text{(S13)}$$

$$x(t_j) = \left(X(t_j), X(t_j - \tau), \ldots, X(t_j - (E-1)\tau)\right) = \left(x_j^{(1)}, \ldots, x_j^{(E+1)}\right), X \in \mathbb{R}, \quad \text{(S14)}$$

We repeat this procedure for every point in the shadow manifold $\boldsymbol{M_Y}$ and keep for each possible pattern $\boldsymbol{P_Y}$ the weighted percentage of the occasions that the contemporaneous predicted dominant pattern $\widehat{P_X}$ equals the real dominant pattern $\boldsymbol{P_X}$. By this procedure, we fill in the PC pattern to pattern matrix (which is illustrated in Tables S1 and S2 for the case of E = 1 and E = 2, respectively):

$$PC[P_X, P_Y] = \sum_t \text{erf}\left(\frac{mean(|S_{y(t)}|)}{mean(|S_{x(t)}|)}\right), \text{ erf: error squashing function.} \quad \text{(S15)}$$

To determine the positive causality, we calculate the average accuracy regarding similar patterns ($\boldsymbol{P_Y}$ is the same as $\boldsymbol{P_X}$):

$$PC(Positive) = \frac{1}{L}\sum diag_{main}(PC), PC(Positive) \in [0, 1]. \quad \text{(S16)}$$

Whereas for the extraction of negative causality, we calculate the average accuracy regarding opposite patterns ($\boldsymbol{P_Y}$ is the opposite of $\boldsymbol{P_X}$):

$$PC(Negative) = \frac{1}{L}\sum diag_{counter}(PC), PC(Negative) \in [0, 1]. \quad \text{(S17)}$$

Dark causality is the average accuracy regarding all the other combinations of patterns between $\boldsymbol{P_Y}$ and $\boldsymbol{P_X}$:

$$PC(Dark) = \frac{1}{L}\sum\left(PC \notin \left(diag_{main}(PC) \cup diag_{counter}(PC)\right)\right), PC(Dark) \in [0, 1]. \quad \text{(S18)}$$

Model dynamical systems and datasets of real applications

In this section, we provide details regarding the models and datasets in the main text. Section a) contains specifications of the models we used, b) contains information regarding the analysis of real applications.

a) Model systems

The models described below are inspired from elementary Lotka-Volterra models studied in [42].

(i) Positive causality system (Figure 2A)

Figure 2A demonstrates the phenomenon of ecological mutualism between two species derived from the following equations:

$$X(t+1) = 0.2X(t)[1 - X(t)/K_X + \varphi(p)0.1\,Y(t)/K_X], X \in \mathbb{R}^+, K_X \in \mathbb{R}^+.$$

$$Y(t+1) = 0.2Y(t)[1 - Y(t)/K_Y + \varphi(p)0.2\,X(t)/K_Y], Y \in \mathbb{R}^+, K_Y \in \mathbb{R}^+. \quad \text{(S19)}$$

K_X and K_Y are the carrying capacities of species *X* and *Y* respectively, in our case both equal to 100. $\varphi(p)$ is a threshold function which is equal to 1 if *p* is greater or equal than 0.5 or 0 if otherwise, with *p* taking a random value between 0 and 1 for each *t*. The rationale behind $\varphi(p)$ is to make the model more realistic by having the two species not interacting in every turn. The starting conditions are: $X(1) = 10$, $Y(1) = 5$, and we use $E = 2$, $\tau = 1$, $L = 200$.

(ii) Negative causality system (Figure 2B)

Figure 2B demonstrates the phenomenon of ecological competition between two species derived from the following equations:

$$X(t+1) = 0.7X(t)[1 - X(t)/K_X - \varphi(p)0.2\,Y/K_X], X \in \mathbb{R}^+, K_X \in \mathbb{R}^+.$$

$$Y(t+1) = 0.7Y(t)[1 - Y(t)/K_Y + \varphi(p)0.3\,X/K_Y], Y \in \mathbb{R}^+, K_Y \in \mathbb{R}^+. \quad \text{(S20)}$$

K_X and K_Y are the carrying capacities of species *X* and *Y* respectively, in our case both equal to 100. $\varphi(p)$ is a threshold function which is equal to 1 if *p* is greater or equal than 0.5 or 0 if otherwise, with *p* taking a random value between 0 and 1 for each *t*. The rationale behind $\varphi(p)$ is to make the model more realistic by having the two species not interacting in every turn. The starting conditions are: $X(1)=50$, $Y(1)=50$ and we use $E = 2$, $\tau = 1$, $L = 200$.

(iii) Dark causality system (Figure 2C)

Figure 2C displays the relationship between two species of prey *X* and *Y* that act as scapegoat to each other under the presence of a common predator *Z*. Such a system is described by the following equations:

$$X(t+1) = -\varphi_{XZ}(p)0.002X(t)Z(t) + \varphi_X(p)0.2X(t)\left(K_X - X(t)\right)/K_X, X \in \mathbb{R}^+, K_X \in \mathbb{R}^+.$$

$$Y(t+1) = -\varphi_{YZ}(p)0.002Y(t)Z(t) + \varphi_Y(p)0.2Y(t)\left(K_Y - Y(t)\right)/K_Y, Y \in \mathbb{R}^+, K_Y \in \mathbb{R}^+. \quad \text{(S21)}$$

$$Z(t+1) = -0.2Z(t) + \varphi_{XZ}(p)0.005X(t)Z(t) + \varphi_{YZ}(p)0.010Y(t)Z(t), Z \in \mathbb{R}^+, K_Z \in \mathbb{R}^+.$$

K_X *and* K_Y are the carrying capacities of species *X* and *Y* respectively, in our case both equal to 100. $\varphi_{XZ}(p)$, $\varphi_X(p)$, $\varphi_{YZ}(p)$ and $\varphi_Y(p)$ are threshold functions.

- $\varphi_{XZ}(p)$ is equal to 1 if *p* is between 0.666 and 1 or 0 if otherwise
- $\varphi_X(p)$ is equal to 1 if *p* is between 0.166 and 0.333 or 0 if otherwise
- $\varphi_{YZ}(p)$ is equal to 1 if *p* is between 0.333 and 0.666 or 0 if otherwise
- $\varphi_Y(p)$ is equal to 1 if *p* is between 0 and 0.166 or 0 if otherwise

with *p* taking a random value between 0 and 1 for each *t*. The rationale behind $\varphi_{XZ}(p)$, $\varphi_X(p)$, $\varphi_{YZ}(p)$ and $\varphi_Y(p)$ is to make the model more realistic by having the species not interacting in every turn. Besides a prey species (say *X*) is more likely to breed when the other prey species (say *Y*) are hunted in their place, as scapegoats, by the common predator. The starting conditions are: $X(1)=100$, $Y(1)=100$, $Z(1)=50$ and we use $E = 2$, $\tau = 1$, $L = 200$.

b) Real applications

(i) A pair of equities (Figures 3A-B)

In Figures 3A-B we demonstrate the application of PC on daily time series data of Apple (AAPL) and Microsoft (MSFT) equities. The data are retrieved via Thomson Reuters Datastream. The time span is from 1986-3-13 to 2018-8-6. The parameters we use are $E = 3$, $\tau = 1$, $L = 8000$.

(ii) Stock market performance versus government bond yield (Figures 3C-D)

In Figures 3C-D we demonstrate the application of PC to the pair of S&P 500 (as a proxy of stock market performance) and U.S. government 10-year bond yield. The data are retrieved via Thomson Reuters Datastream. The time span is from 1985-1-2 to 2018-8-6. The parameters we use are $E = 3$, $\tau = 1$, $L = 8000$.

(iii) Complex financial network of sovereign CDS (Figures 4A-I)

The sovereign CDS data we used to analyze with PC are from the following countries: Argentina, Tunisia, Venezuela, Czech Republic, Dominican Republic, Germany, Brazil, France, Greece, Hong Kong, Ireland, Jamaica, Japan, Bahrain, Belgium, Denmark, Norway, Spain, Sweden, Thailand, Netherlands, Lebanon, Malaysia, New Zealand, Uruguay, China, Austria, Bulgaria, Chile, Colombia, Costa Rica, Croatia, Cyprus, El Salvador, Estonia, Guatemala,

Hungary, Iceland, Indonesia, Iraq, Italy, Kazakhstan, Latvia, Lithuania, Malta, Panama, Peru, Poland, Portugal, Serbia, Singapore, Slovenia, South Africa, Philippines, Turkey, Romania, Russia, Slovakia, Vietnam, Israel, Qatar, Ukraine, U.K., Mexico, Finland, South Korea, Morocco, U.S.A., Australia. The data are retrieved via Thomson Reuters Datastream. The time span is from 2010-5-4 to 2018-8-6. The parameters we use are: $E = 3$, $\tau = 1$, $L = 1000$.

(iv) Predator-prey interactions in the Didinium-Paramecium system (Figures S6A-B)

Next, we apply PC on experimental time series from the classical Didinium-Paramecium system. For a thorough description of the experimental conditions refer to the supplementary material of[13]. The data analyzed can be found at http://robjhyndman.com/tsdldata/data/veilleux.dat. The first 10 data points were removed to eliminate transient behavior in the initial period of the experiment. The parameters we use are: $E = 3$, $\tau = 1$. To account for the limited length of time series, we used leave-one-out cross validation for the PC analysis.

(v) Complex ecosystem of Sardine-Anchovy-SST (Figures S6C-F)

This dataset was also studied by[13] and details are also found in their supplementary material. Sea surface temperature (SST) data are available from: http://shorestation.ucsd.edu/active/index_active.html). Landings data for sardine and anchovy were taken from two sources: 1. (1928-2002) NOAA Southwest Fisheries Science Center (http://las.pfeg.noaa.gov:8080/las_fish1/servlets/dataset?catitem=2) 2. (2003-2006) California Department of Fish and Game (http://www.dfg.ca.gov/marine/landings05.asp). The parameters we use are $E = 3$, $\tau = 1$. To address the limited length of time series, we used leave-one-out cross validation was used for the analysis.

(vi) Complex physiological system of heart-lungs-blood oxygen concentration (Figures S7A-F)

This dataset was used in the Santa Fe time series competition as Dataset B and was also studied by[12]. The dataset consists of heart rate, breath rate and blood oxygen concentration time series from a patient in the Beth Israel Deaconess Medical Center in Boston, Massachusetts[43]. Details about the dataset and very dataset can be found in https://www.physionet.org/physiobank/database/santa-fe/. The parameters we use are $E = 3$, $\tau = 1$, $L = 1000$.

Figure S1.

Pearson cross correlation for the three models of positive (Eq. S19), negative (Eq. S20) and dark causality (Eq. S21). As we can see correlation is unstable for the case of competitive variables (Fig. S1B) and is completely irrelevant (by design) for the case of dark causality (Fig. S1C) by taking positive fluctuating values.

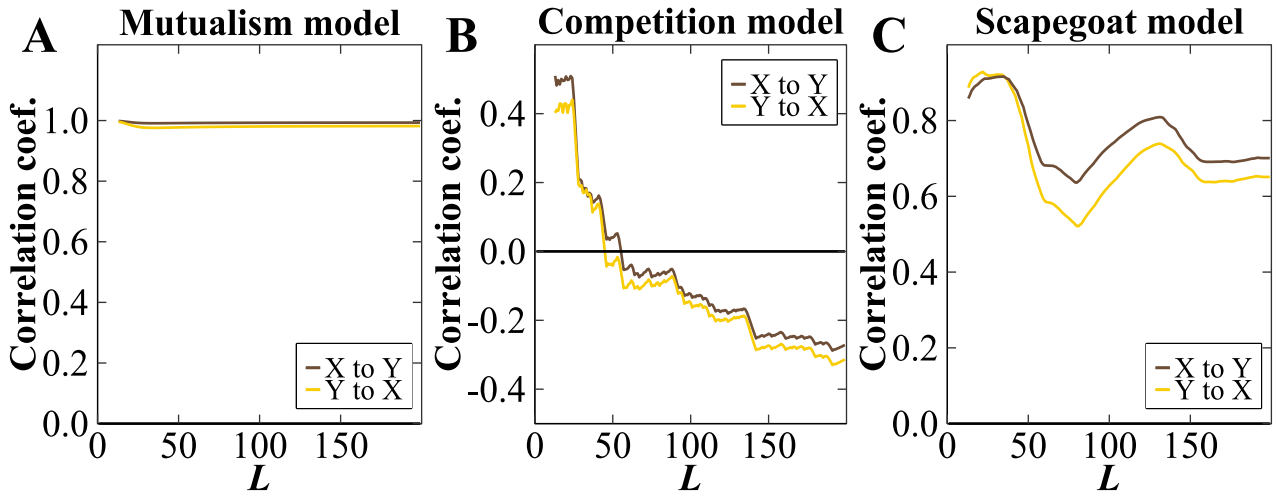

Fig. S1. Correlation is not causality, and dark causality is a case completely unapproachable by correlation. (A) Correlation between X and Y from positive causality model in Eq. S19. (B) Correlation between X and Y from negative causality model in Eq. S20. (C) Correlation between X and Y from dark causality model in Eq. S21.

Figure S2.

Beta coefficient of cointegration for the three models of positive (Eq. S19), negative (Eq. S20) and dark causality (Eq. S21). The coefficient of cointegration is unstable for the case of competitive variables (Fig. S2B) and cannot by default uncover any meaningful result for the case of dark causality (Fig. S2C).

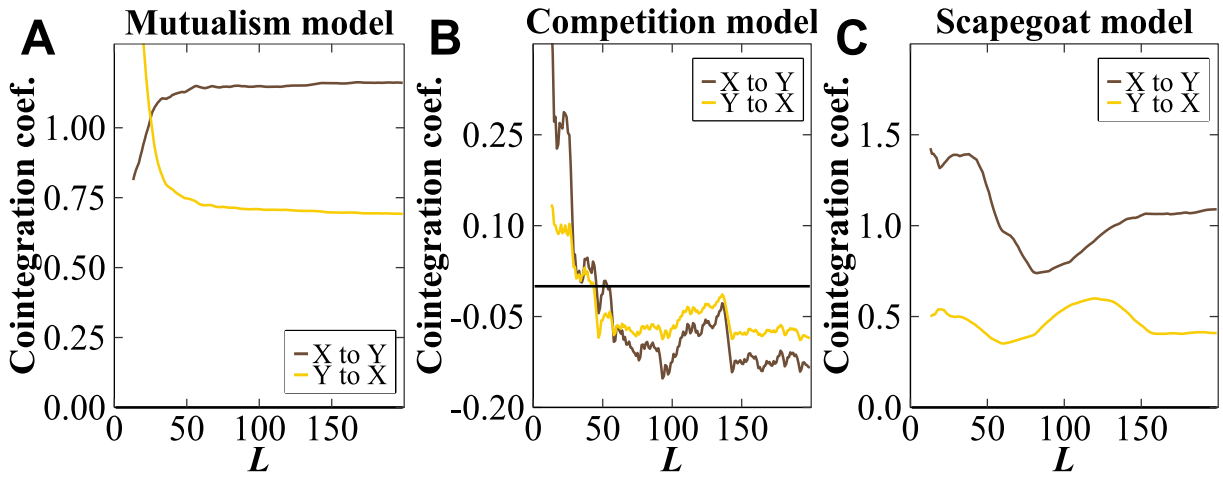

Fig. S2. Dark causality is a case out of the radar for cointegration. (A) Coefficient of cointegration between *X* and *Y* from positive causality model in Eq. S19. (B) Coefficient of cointegration between *X* and *Y* from negative causality model in Eq. S20. (C) Coefficient of cointegration between *X* and *Y* from dark causality model in Eq. S21.

Figure S3.

S-map interactions for the three models of positive (Eq. S19), negative (Eq. S20) and dark causality (Eq. S21). For the case of positive causality S-map captures clearly the influence from *X* to *Y* but is unstable from *Y* to *X*. In the case of negative causality S-map is unstable yet yields towards the negative side. Similar to the cases of correlation and cointegration, S-map is not designed to capture forms of dark causality (Fig. S3C).

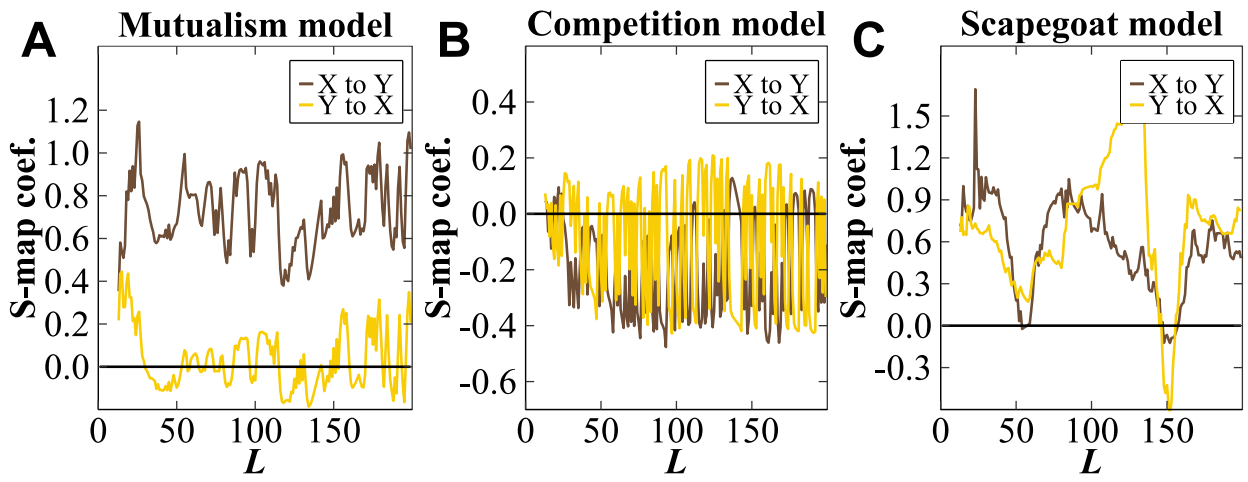

Fig. S3. S-map is not designed to quantify cases of dark causality. (A) S-map interaction between *X* and *Y* from positive causality model in Eq. S19. (B) S-map interaction between *X* and *Y* from negative causality model in Eq. S20. (C) S-map interaction between *X* and *Y* from dark causality model in Eq. S21.

Figure S4.

Pattern Causality for the three models of positive (Eq. S19), negative (Eq. S20) and dark causality (Eq. S21) demonstration.

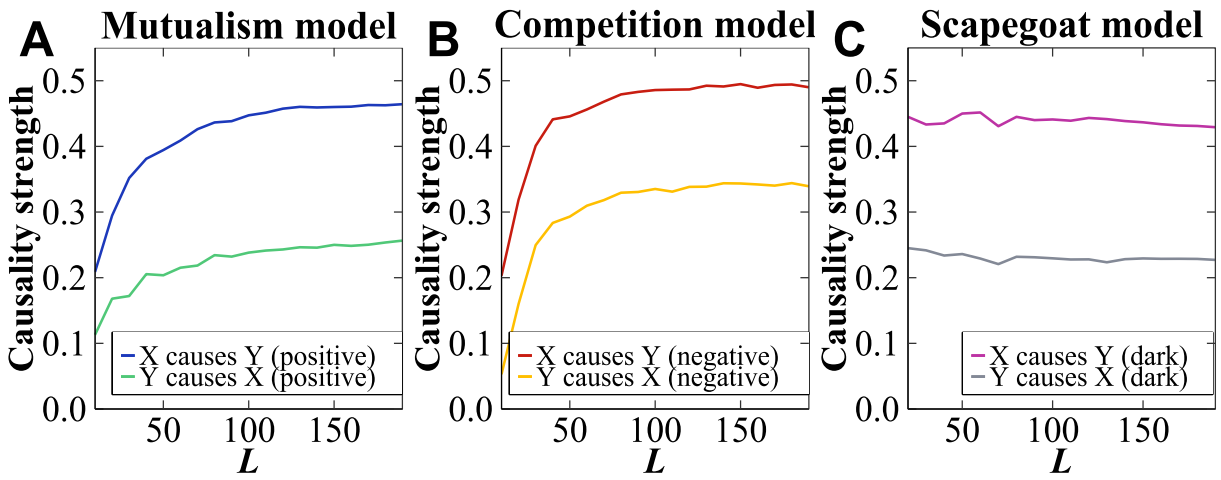

Fig. S4. Pattern Causality is designed to quantify the intensity of positive, negative and dark causal interactions. (A) PC between X and Y from positive causality model in Eq. S19. (B) PC between X and Y from negative causality model in Eq. S20. (C) PC between X and Y from dark causality model in Eq. S21. Color scheme: Blue and green are used for positive causality. Red and yellow are used for negative causality. Purple and grey are used for dark causality.

Supplementary examples for ecology and physiology

Predator – prey dynamics. To explore the nature of causality in predator – prey relations we implement PC in the standard experimental system of *Didinium* (predator) and *Paramecium* (prey)[44] (Fig. S6A). CCM analysis showed[13] that this pair of species is characterized by bidirectional causality, with causation from predator to prey being stronger than reversely.

Our results foster the top-down control from predator to prey but moreover PC displays a verbose explanation of predator-prey interactions. Fig. S6B reveals the distinctly negative causality from *Didinium* to *Paramecium*. This outcome is rational considering that as the predator population rises more prey gets consumed and thus prey population diminishes. Furthermore, notice that positive causality is stronger from prey to predator, which is expected if we consider that when prey population surges this supplies the predators with more to consume.

Hidden interactions in a simple ecosystem. Next, we investigate an ecosystem consisting of anchovy and sardine landings (Fig. S6C), and sea surface temperature (SST) measured at Newport Pier and Scripps Pier, California. Such ecosystems have been a subject of conflicting analyses and mirage correlations[45, 46]. Some[47] suggest that the species are in direct competition, others[48] claim that the species' interaction are indirectly influenced by shared environmental forcing. CCM analysis[13] showed that the only causal role is that of SST influencing sardine and anchovy landings.

PC analysis exposes a complex interaction among sardines and anchovies (see Fig. S6D). This dark causality could possibly attest to the fact that there is controversy in the literature regarding their actual interaction[47-49]. Furthermore, we can see that causality from SST to sardines and anchovies is also of dark nature (see Fig. S6E, S6F). Therefore, we can deduce that temperature at sea level influences anchovies and sardines though in an intricate manner, neither purely beneficial nor harmful.

Overall our results suggest that apart from a dynamic (state-dependent) rule involving temperature (already advocated in [13]), acute management decisions should also be based upon closer monitoring of more subtle species interactions than obvious predation and symbiosis (e.g. resources competition).

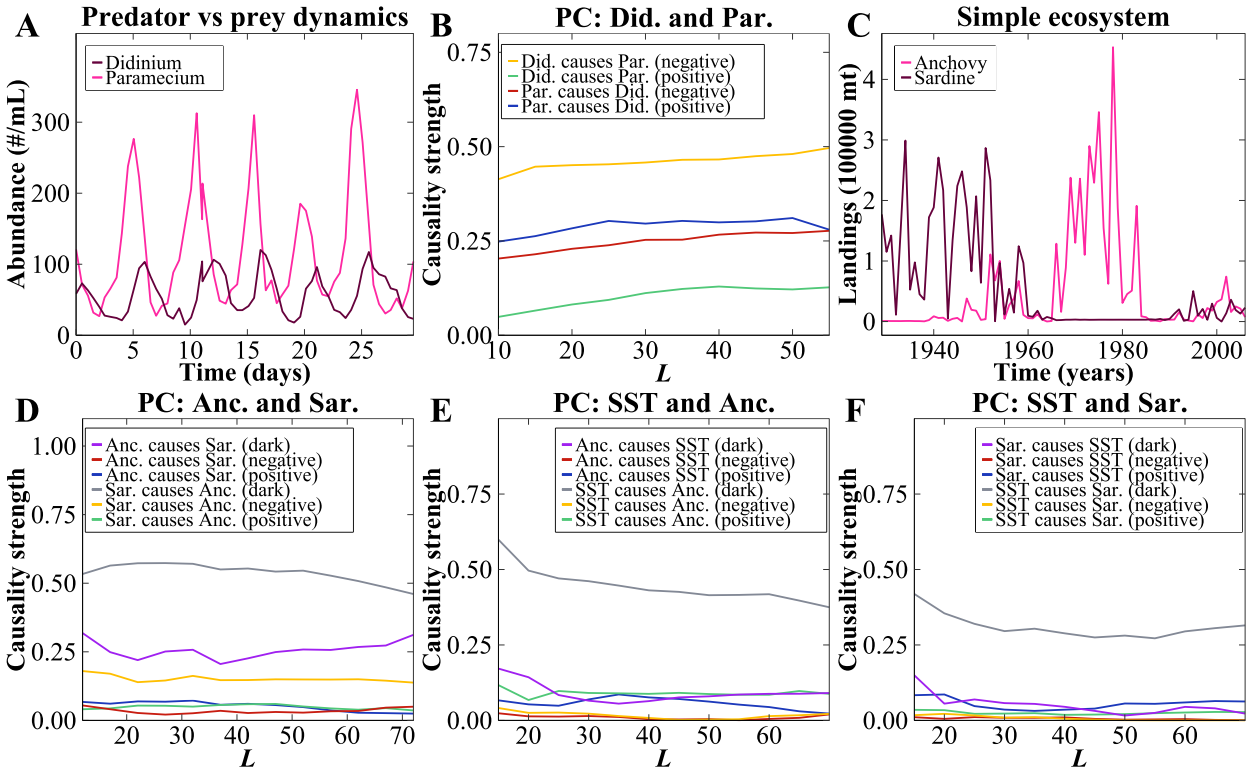

Fig. S6. Nature of causality in ecological data. (**A**) Abundance time series of *Didinium* and *Paramecium*. (**B**) PC exposes their mostly negative interaction. (**C**) Landings time series of anchovy and sardine. (**D** to **F**) Dark causality from SST towards both species as well as between the two species. **Color scheme**: Blue and green are used for positive causality. Red and yellow are used for negative causality. Purple and grey are used for dark causality.

Vital synergies in an apnea patient. Physiological research focuses a lot on cardio – respiratory interplays to understand certain diseases[50]. Sleep apnea is one of them and is severe because it causes sleep deprivation and ultimately death[43]. We investigate causal interactions among heart rate, breath rate and blood oxygen concentration (Fig. S7 A to C) from a patient in the Beth Israel Deaconess Medical Center in Boston, Massachusetts[43]. The same dataset was studied by Schreiber[12] (without considering blood oxygen concentration) and he found information transfer to be stronger from heart to breath rate than vice versa.

By employing PC, we find that heart rate regulates breath rate in a complex way (Fig. S7D. Blood oxygen concentration and heart rate are involved in a mixed (positive and negative) causal loop (see Fig. S7E) with blood oxygen concentration yielding a stronger influence. However, the influence from blood oxygen concentration to breath rate (see Fig. S7F) is unilateral and of a mostly dark nature.

Our results move one step beyond Schreiber's conclusions highlighting heart rate's dominant role over breath rate (see Fig. S7D), and moreover unveiling the nature of their interaction. All in all, blood oxygen concentration seems to be highly influential in the cardio – respiratory dynamics and should not be neglected by medical research on apnea.

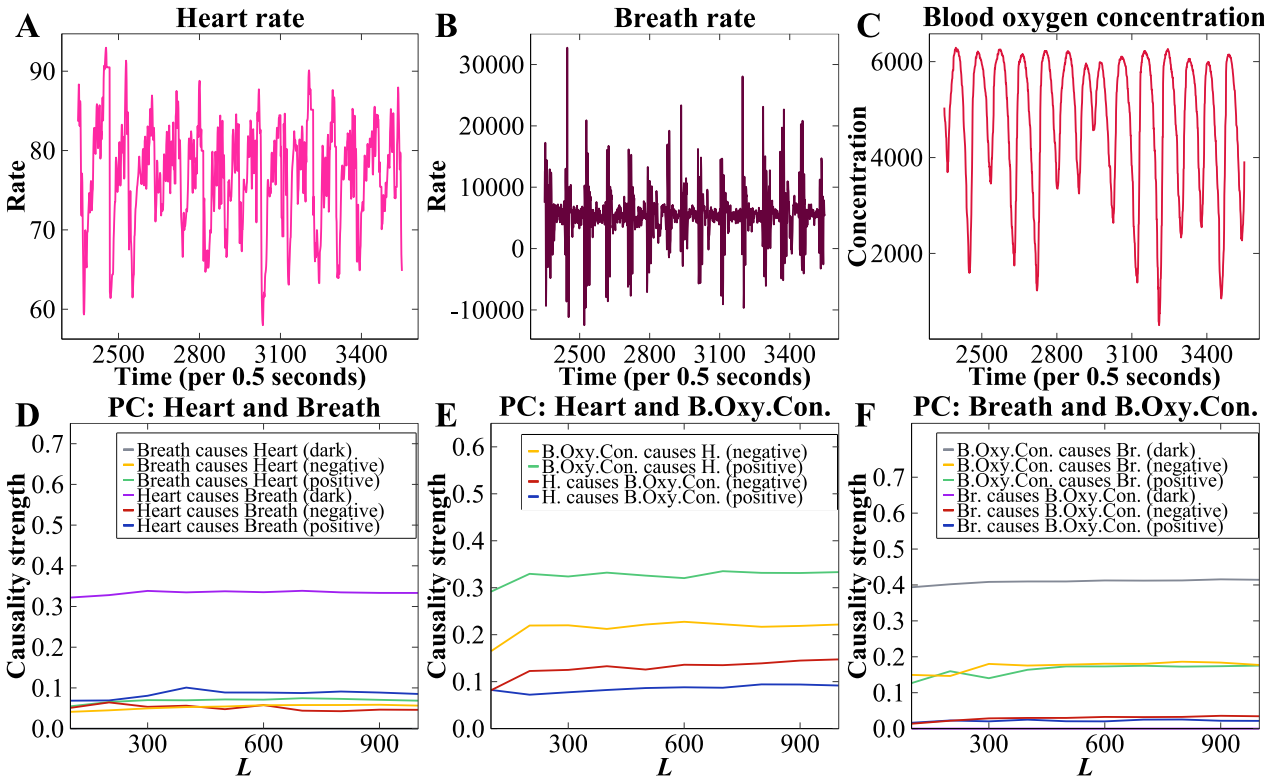

Fig. S7. Nature of causality in physiological data of a patient with apnea. (**A**) Time series of heart rate (**B**), breath rate (**C**) and blood oxygen concentration. (**D**) Unilateral influence from heart rate towards breath rate (**E, F**) PC reveals the dominant causal role of blood oxygen concentration which exerts both positive and negative causality to heart and breath rate. **Color scheme**: Blue and green are used for positive causality. Red and yellow are used for negative causality. Purple and grey are used for dark causality.

Table S1.

PC (from *X* to *Y*) pattern to pattern matrix for $E = 2$. Each cell is filled with the weighted accuracy (percentage) regarding the occasions when given an average pattern in *Y*'s neighborhood we successfully predict the average pattern in *X*'s contemporaneous neighborhood. Thus, each cell takes values from 0 to 1. To calculate positive causality, we take the average of blue cells. For negative causality we take the average weighted accuracy inside red cells. Dark causality is the average weighted accuracy inside the purple cells.

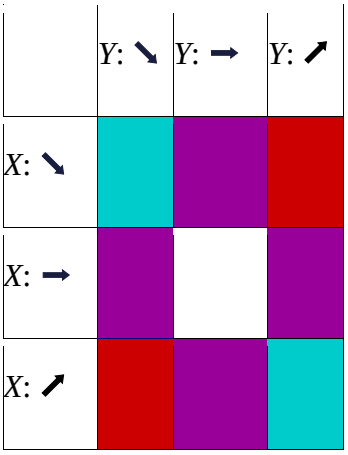

Table S2.

PC (from *X* to *Y*) pattern to pattern matrix for $E = 3$. Each cell is filled with the weighted accuracy (percentage) regarding the occasions when given an average pattern in *Y*'s neighborhood we successfully predict the average pattern in *X*'s contemporaneous neighborhood. Thus, each cell takes values from 0 to 1. To calculate positive causality, we take the average of blue cells. For negative causality, we take the average weighted accuracy inside red cells. Dark causality is the average weighted accuracy inside the purple cells.

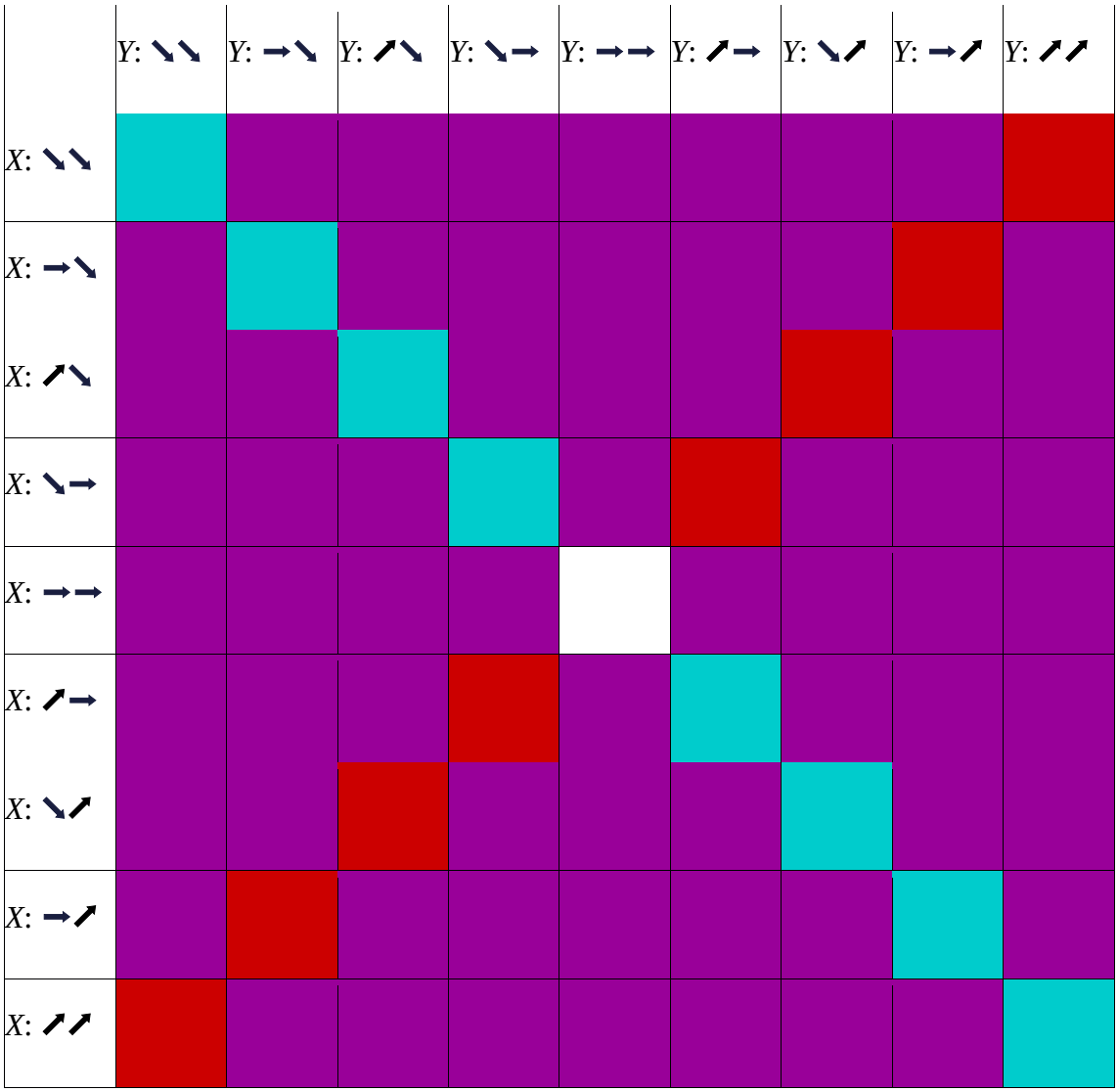

SI Video

This video demonstrates the extraction of the nature of causality between time series.

References

1. Gai, P. and Kapadia, S., Contagion in financial networks. In *Proceedings of the Royal Society of London A: Mathematical, Physical and Engineering Sciences*, **466**, 2401-2423 (2010).

   doi: 10.1098/rspa.2009.0410

2. Preis, T., Schneider, J.J. and Stanley, H.E., Switching processes in financial markets. *Proceedings of the National Academy of Sciences*, **108**(19), 7674-7678 (2011). doi:10.1073/pnas.1019484108

3. Gabaix, X., Gopikrishnan, P., Plerou, V. and Stanley, H.E., A theory of power-law distributions in financial market fluctuations. *Nature*, **423**, 267-270 (2003).

   doi:10.1038/nature01624

4. Boginski V., Butenko S. and Pardalos P.M., Statistical analysis of financial networks. *Computational Statistics & Data Analysis*, **48**(2), 431-443 (2005).

   doi:10.1016/j.csda.2004.02.004

5. Preis, T., Reith, D. and Stanley, H.E., Complex dynamics of our economic life on different scales: insights from search engine query data. *Philosophical Transactions of the Royal Society of London A: Mathematical, Physical and Engineering Sciences*, **368***(1933)*, 5707-5719 (2010).

   doi:10.1098/rsta.2010.0284

6. Markowitz H., Portfolio selection, *The Journal of Finance,* **7**(1), 77-91 (1952).

   doi:10.1111/j.1540-6261.1952.tb01525.x

7. Yule G. U., Why do we sometimes get nonsense-correlations between time-series? A study in sampling and the nature of time-series. *Journal of the Royal Statistical Society,* **89**, 1-63 (1926).

   doi:10.2307/2341482

8. Pearson K., Notes on regression and inheritance in the case of two parents. *Proceedings of the Royal Society of London,* **58**, 240-242 (1895).

   doi:10.1098/rspl.1895.0041

9. Pearl J., *Causality: models, reasoning, and inference* (Cambridge University Press, 2009).

10. Granger C. W. J., Investigating causal relations by econometric models and cross-spectral methods. *Econometrica,* **37**(3), 424-438 (1969).

doi:10.2307/1912791

11. Engle R.F. and Granger C.W., Co-integration and error correction: representation, estimation, and testing. *Econometrica*, **55**(2), 251-276 (1987).

doi:10.2307/1913236

12. Schreiber T., Measuring information transfer. *Physical Review Letters,* **85**, 461 (2000).

doi:10.1103/PhysRevLett.85.461

13. Sugihara G., May R., Ye H., Hsieh C.H., Deyle E., Fogarty M. and Munch S., Detecting causality in complex ecosystems. *Science,* **338**, 496-500 (2012).

doi:10.1126/science.1227079

14. Deyle E.R., May R.M., Munch S.B. and Sugihara G., Tracking and forecasting ecosystem interactions in real time. *Proceedings of the Royal Society B: Biological Sciences*, **283**(1822), 2015-2258 (2016).

doi:10.1098/rspb.2015.2258

15. Gatev, E., Goetzmann, W.N. and Rouwenhorst, K.G., Pairs trading: Performance of a relative-value arbitrage rule. *The Review of Financial Studies*, **19**(3), 797-827 (2006).

doi:10.1093/rfs/hhj020

16. Chow, G., Jacquier, E., Kritzman, M. and Lowry, K., Optimal portfolios in good times and bad. *Financial Analysts Journal*, **55**(3) 65-73 (1999).

doi:10.2469/faj.v55.n3.2273

17. Morse M. and Hedlund G.A., Symbolic dynamics. *American Journal of Mathematics,* **60**(4), 815-866 (1938).

doi: 10.2307/2371264

18. Takens F., Detecting strange attractors in turbulence. In: Rand D., Young LS. (eds) *Dynamical Systems and Turbulence*, Warwick 1980. Lecture Notes in Mathematics, vol. **898**. Springer, Berlin, Heidelberg, 366-381 (1981).

doi:10.1007/BFb0091924

19. Deyle E.R. and Sugihara G., Generalized theorems for nonlinear state space reconstruction. *PLoS ONE* **6**, e18295 (2011).

doi:10.1371/journal.pone.0018295

20. See supplementary materials.

21. Crespi B.J., Vicious circles: positive feedback in major evolutionary and ecological transitions. *Trends in Ecology & Evolution,* **19**, 627-633 (2004).

doi:10.1016/j.tree.2004.10.001

22. Hall, J.E., *Guyton and Hall textbook of medical physiology*, Elsevier Health Sciences (2015).

23. Arthur W.B., Positive feedbacks in the economy. *Scientific American,* **262**(2), 92-99 (1990).

24. Neutel A.M., Heesterbeek J.A., Van de Koppel J., Hoenderboom G., Vos A., Kaldeway C., Berendse F. and De Ruiter P.C., Reconciling complexity with stability in naturally assembling food webs. *Nature,* **449**, 599-602 (2007).

doi:10.1038/nature06154

25. Raven P.H. and Johnson G.B., *Biology*, Boston: Hill Companies Inc. USA (1999).

26. Prechter Jr R.R., Unconscious herding behavior as the psychological basis of financial market trends and patterns. *The Journal of Psychology and Financial Markets,* **2**, 120-125 (2001).

doi:10.1207/S15327760JPFM0203_1

27. Da Z., Engelberg J. and Gao P., In search of attention. *The Journal of Finance,* **66**(5), 1461-1499 (2011).

doi:10.1111/j.1540-6261.2011.01679.x

28. Kwan S.H., Firm-specific information and the correlation between individual stocks and bonds. *Journal of Financial Economics,* **40**(1), 63-80 (1996).

doi:10.1016/0304-405X(95)00836-4

29. Gündüz Y. and Kaya, O., Impacts of the financial crisis on eurozone sovereign CDS spreads. *Journal of International Money and Finance,* **49**(Part B), 425-442 (2014).

doi:10.1016/j.jimonfin.2014.03.013

30. Peltonen T.A., Scheicher M. and Vuillemey G., The network structure of the CDS market and its determinants. *Journal of Financial Stability,* **13**, 118-133 (2014).

doi:10.1016/j.jfs.2014.05.004

31. Acharya V., Philippon T., Richardson M. and Roubini N., The financial crisis of 2007-2009: Causes and remedies. *Financial Markets, Institutions & Instruments,* **18**(1), 89-137 (2009).

doi:10.1111/j.1468-0416.2009.00147_2.x

32. Hamilton E., Cairns H., Cooper L., The collected dialogues of Plato (Princeton University Press, 1961).

33. Hennig B., The four causes. The Journal of Philosophy 106, 137-160 (2009). doi:10.5840/jphil200910634

34. Bandt C., Pompe B., The entropy profile - A function describing statistical dependences. *Journal of Statistical Physics* **70**(3-4), 967-983 (1993).

doi.org/10.1007/BF0105360

35. Bandt C., Pompe B., Permutation entropy: a natural complexity measure for time series. *Physical Review Letters* **88**(17), 174102 (2002).

doi:10.1103/PhysRevLett.88.174102

36. Alligood T.K., Sauer T.D., Yorke J.A., *Chaos. An introduction to dynamical systems* (Springer Verlag, 2000).

37. Josic K., Synchronization of chaotic systems and invariant manifolds. *Nonlinearity* **13**, 1321 (2000).

38. Crutchfield J.P., thesis, University of California, Santa Cruz (1979).

39. Ruelle D., *Chaotic Evolution and Strange Attractors: The Statistical Analysis of Time Series for Deterministic Nonlinear Systems* (Cambridge Univ. Press, Cambridge, 1989).

40. Trimble V., Existence and nature of dark matter in the universe. *Annual Review of Astronomy and Astrophysics*, **25**(1), 425-472 (1987).

doi:10.1146/annurev.aa.25.090187.002233

41. Krakovská A., Mezeiová K., Budáčová H., Use of false nearest neighbours for selecting variables and embedding parameters for state space reconstruction. *Journal of Complex Systems*, (2015), Article ID 932750, 12 pages.

doi:10.1155/2015/932750

42. Edelstein-Keshet L., *Mathematical Models in Biology* (SIAM, 2004).

doi:10.1137/1.9780898719147

43. Rigney D.R., Goldberger A.L., Ocasio W., Ichimaru Y., Moody G.B., and Mark R., in Time Series Prediction: Forecasting the Future and Understanding the Past, edited by A. Weigend S. and Gershenfeld N. A. (Addison-Wesley, Reading, MA, 1993).

44. Luckinbill L.S., Coexistence in laboratory populations of Paramecium aurelia and its predator Didinium nasutum. *Ecology* **54**, 1320 (1973).

doi: 10.2307/1934194

45. Jacobson L.D., MacCall A.D., Stock-recruitment models for Pacific sardine (Sardinops sagax). *Canadian Journal of Fisheries and Aquatic Sciences* **52**, 566 (1995).

doi:10.1139/f95-057

46. McClatchie S., Goericke R., Auad G., Hill K., Re-assessment of the stock-recruit and temperature-recruit relationships for Pacific sardine (Sardinops sagax). *Canadian Journal of Fisheries and Aquatic Sciences* **67**, 1782 (2010).

doi:10.1139/F10-101

47. Murphy G.I., Isaacs J.D., Species replacement in marine ecosystems with reference to the California current. *Minutes of Meeting Marine Research Committee 7*, 1 (1964).

48. Lasker R., MacCall A., in *Proceedings of the Joint Oceanographic Assembly, Halifax, August 1982: General Symposia* (Department of Fisheries and Oceans, Ontario, 1983), pp. 110–120.

49. Patil D.A.S., Hunt B.R., Carton J.A., Identifying low-dimensional nonlinear behavior in atmospheric data. *Monthly Weather Review* **129**, 2116 (2001).

doi:10.1175/1520-0493(2001)129<2116:ILDNBI>2.0.CO;2

50. Hirsch J.A., Bishop B., Respiratory sinus arrhythmia in humans: how breathing pattern

modulates heart rate. *American Journal of Physiology-Heart and Circulatory Physiology* **241**, H620-H629 (1981).

doi:10.1152/ajpheart.1981.241.4.H620